mDixon-Based Synthetic CT Generation via Patch Learning

Xin Song[1,2], Jiamin Zheng[1,2], Chao Fan[1,2], and Hongbin Yu[1,2(✉)]

[1] School of Digital Media, Jiangnan University, Wuxi 214122, China
1785613841@qq.com
[2] Jiangsu Key Laboratory of Media Design and Software Technology, Jiangnan University, Wuxi 214122, China

Abstract. We proposed a new method for generating synthetic CT on abdomen from modified Dixon (mDixon) MR data of abdomens to address the challenges of PET/MR attenuation correction (AC). AC is necessary in process of PET/MR but MR data lack photon attenuation, thus multiple methods are proposed to generate synthetic CT. However, these existing methods requires advantaged MR sequences which needs fine acquisition and huge cost consumption. To address this problem, we proposed a new method for generating synthetic CT using Patch Learning (SCG-PL). Global model of SCG-PL is transfer learning and patch model is semi-supervised classification. The advantages of our method can be summarized into two points. (1) Patch learning is a gradual learning process with gradually updating global model on remodeling patch model, so our SCG-PL method is gradually capable of generating synthetic CT. (2) Semi-supervised classification adopted in the process of patch learning, only small amount of labeled data is needed in SCG-PL, which greatly reduced the workload of radiologists. The experimental results indicate that proposed SCG-PL method can effectively generate synthetic CT image from challenging abdomen images using mDixon MR sequence data only.

Keywords: Synthetic CT generation · mDixon-based MR · Abdomen · Attenuation correction (AC) · Patch learning (PL)

1 Introduction

Benefit from the superior soft tissue contrast and high anatomical resolution, Magnetic Resonance Imaging (MRI) scans have been widely applied in radiotherapy [1, 2]. With the evolution of modern medical imaging technologies, PET/MR, combining with advantages of two imaging modalities, can offer further information which cannot be presented in PET/CT and has potential applications. Meanwhile, compared with CT, the characteristic of using no ionizing radiation MRI has an absolute advantage. Yet there are rarely MRI or PET/MR used in radiotherapy procedure individually due to the lack of the geometric integrity and precision in mapping Relative Electron Density (RED) for dose calculations.

Solely using MRI or PET/MR for radiotherapy has become an interesting goal in radioactive medicine. Here, the primary problem to be solved is attenuation correction

Y.-D. Zhang et al. (Eds.): ICMTEL 2020, LNICST 327, pp. 411–421, 2020.
https://doi.org/10.1007/978-3-030-51103-6_37

in radiotherapy. To achieve this goal, multiple methods are proposed. However, the diversity and the real-time movement of human organs and tissues directly cause the failure of methods, such as atlas-based [3, 4] and template-based [5]. Standing out from the proposed methods, the synthetic CT generation method by distinguishing the tissue type of all voxel in MRI images.

At present, the limitations of the development of synthetic CT generation lie primarily in two areas, i.e. target body sections and methods of generation. From the site of body sections, most studies have focused on brain and breast, these body sections have common characteristic of simple organization and less deformation. Abdomen, as the challenging body section, with its complex anatomical structure and along with a large amount of organs deformation caused by massive human respiration is little studied. From the existing methods, some advantage sequences which are technically challenging like Ultrashort Echo Time (UTE) and Zero Echo Time (ZTE) are needed [6, 7].

Focusing on abdomen, on the basis of existing methods, we introduce the ensemble learning thought i.e. patch learning [8] to generate synthetic CT in the case of only using easily obtainable MR sequence. Global model of SCG-PL is transfer learning and patch model is semi-supervised classification. The advantage of our proposed synthetic CT generation on abdomen using patch learning method (SCG-PL for short) lies mainly in the following two points:

1) The combination of transfer learning and semi-supervised classification in patch learning enables the indistinguishable tissue type i.e. bone, to be well differentiated from voxels of Dixon sequence.
2) With the semi-supervised classification adopted in the process of patch learning, only small amount of labeled data is needed in SCG-PL, which greatly reduced the workload of radiologists.

The rest of this manuscript shows you our proposed SCG-PL method in detail. Related work is introduced in Sect. 2. Specifically, the method is explained in Sect. 3. Section 4 presents the experimental studies. Conclusion is given in Sect. 5.

2 Related Work

2.1 Patch Learning

Patch learning (PL) [8] is a strategy of gradually improving the performance of a machine learning model by iteratively updating the global model by remodeling the patch model. PL consists of the following three steps:

1) Train an initial global model using all training data.
2) Identify L patches from the initial global model, which contribute the most to the learning error, and train a (local) patch model for each patch.
3) Update the global model using training data that do not fall into any patch.

PL zooms into those parts that need more work without discarding the initial entire model, and become an excellent model until appropriate amount of patches remodeled, which is shown as Fig. 1.

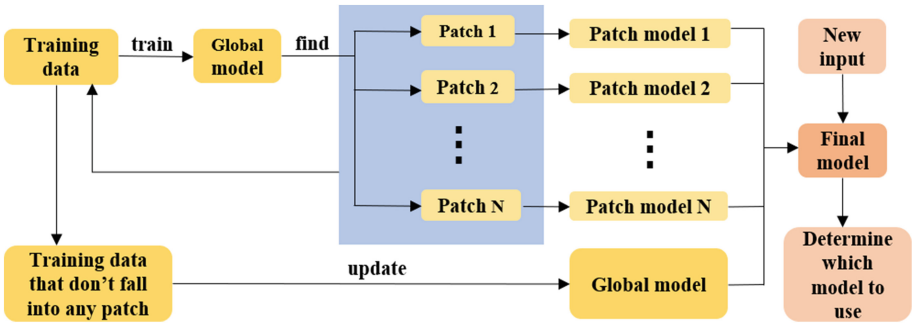

Fig. 1. Idea of PL.

2.2 KT-CM

Fuzzy c-means (FCM) [16] and maximum entropy clustering (MEC) [17] are classical soft partition clustering algorithms that aim to subdivide the data instances in a specific dataset into C pairwise disjointed clusters. Quadratic weights and Gini-Simpson diversity-based fuzzy clustering.

(QWGSD-FC) is an effective soft-partition clustering algorithm, which is intended to simultaneously maintain the advantages of some classical methods. As we all know, conventional soft-partition clustering approaches may not be powerful enough in intricate data circumstances. To address these challenges, based on QWGSD-FC, KT-CM was proposed by combining transfer learning with soft partition clustering. KT-CM offers us sufficient, extra knowledge of the data in the source domain as the prior information, except for the direct information in the target domain.

Let $X_T = \{x_{1,T}, \ldots, x_{N_T,T}\} \in R^{N_T \times d}$ denote the data set in the target domain, where the number of data instances is denoted as N_T and the dimension is denoted as d. C_T represents the number of clusters in the target domain. $U_T = [\mu_{ij,T}]_{C_T \times N_T}$ denotes the generated membership matrix, where the elements indicate the membership degree of the $x_j (j = 1, \ldots, N_T)$ data instance belonging to cluster $i (i = 1, \ldots, C_T)$.

The framework of KT-CM can be reformulated as

$$min\left(J_{KT-CM} = \sum_{i=1}^{C_T}\sum_{j=1}^{N_T}\mu_{ij,T}^2 + \beta\sum_{i=1}^{C_T}\sum_{j=1}^{N_T}\mu_{ij,T}^2 + \gamma\sum_{i=1}^{C_T}\sum_{j=1}^{N_T}\mu_{ij,T}^2\left\|\hat{v}_{i,S} - v_{i,T}\right\|^2\right) \quad (1)$$
$$s.t.\, 0 \le \mu_{ij} \le 1, \sum_{i=1}^{C_T}\mu_{ij} = 1$$

Where $\beta > 0$ denotes the Gini-Simpson diversity measure, $\gamma \ge 0$ represents the transfer optimization parameter, $\hat{v}_{i,S}$ represents the ith cluster centroid in the source domain, and $v_{j,T}$ represents the jth cluster centroid that is estimated in the target domain.

The update of the cluster centroids and fuzzy memberships are as follows

$$v_i = \frac{\sum_{j=1}^{N} \mu_{ij}^2 + \gamma \hat{v}_i \sum_{j=1}^{N} \mu_{ij}^2}{(1+\gamma) \sum_{j=1}^{N} \mu_{ij}^2} \tag{2}$$

$$\mu_{ij} = \frac{1}{\left(2\left\|x_j - v_i\right\|^2 + 2\beta + 2\gamma\|\hat{v}_i - v_i\|^2 \times \sum_{K=1}^{C} \frac{1}{2\left\|x_j - v_k\right\|^2 + 2\beta + 2\gamma\|\hat{v}_K - v_K\|^2}\right)} \tag{3}$$

2.3 Laplacian Support Vector Machine (LapSVM)

LapSVM, a semi-supervised classification algorithm based on manifold regularization, mainly research on how to use a small number of labeled samples and a large number of unlabeled samples for training and classification, which is an extension of the traditional SVM. The LapSVM learning model contains the intrinsic geometry information of the sample because of the introduction of sample manifold regularity item.

Assume the sample set $S = \{x_i,\ i = 1, \ldots, n\}$, x_i represents the ith sample and n represents the number of samples. Set $L = \{x_i, i = 1, \ldots, m\}$ represents the labeled sample, m represents the number of the labeled sample. Set $U = \{x_i, i = 1, \ldots, u\}$ represents the unlabeled sample, u represents the number of the unlabeled sample. Let y_i represent the category of the ith sample, $y_i \in \{-1, 1\}$. The LapSVM model is defined as follows

$$f^* = \underset{f \in H_k}{min} \sum_{i=1}^{m} max(1 - y_i f(x_i), 0) + \gamma_A \|f\|_A^2 + \gamma_I \|f\|_I^2 \tag{4}$$

Where, $f = [f(x_i), x_i \in S]^T$ is an n-dimensional column vector on the training data set. $\|\cdot\|_A^2$ is the Ambient Norm defined in the regenerative nuclear Hilbert space (RKHS), H_k is the RKHS related to the kernel function. Parameter γ_A is weight, which controls the complexity of $\|f\|_A^2$ in RKHS. $\|f\|_I^2$ is the intrinsic regular term, which keeps the inner manifold structure of the sample distribution. Parameter γ_I is the weight of the function in the low-dimensional manifold, which controls the complexity of inner geometry function. By calculating the Lagrangian multiplier, the classifier is as follows

$$f^* = \sum_{i=1}^{n} \alpha_i^* K(x_i, x) \tag{5}$$

Where, α_i^* is the Lagrangian multiplier and K is the kernel matrix. Solving the Lagrangian multiplier

$$\alpha^* = (2\gamma_A I + 2\gamma_I KL)^{-1} J_L^T Y \beta^* \tag{6}$$

Where, I is the identity matrix and L is the Laplacian matrix. $Y \in R^{m\times n}$ is a diagonal matrix composed of identification samples $y_i (i = 1, \ldots, m)$. $J_L \in R^{m\times n}$ is a block matrix $[IO]$ formed by labeled samples and unlabeled samples. β is the Lagrange multiplier, which is

$$\begin{aligned} \beta^* &= \underset{\beta \in R^m}{max} \sum \beta^i - \tfrac{1}{2}\beta^T Q\beta \\ Q &= YJ_L K(2\gamma_A + 2\gamma_I KL)^{-1} J_L^T Y \\ s.t. \sum_{i=1}^{m} \beta_i y_i &= 0; 0 \le \beta_i \le 1, i = 1, \ldots, m \end{aligned} \tag{7}$$

3 The Proposed SSG-PL Method

The proposed SCG-PL method includes data prepare stage, constructing Patch Learning (PL) model and generating synthetic CT image. In data prepare stage, we extract features of four types of MR data to form seven-dimensional MR feature data for each subject and obtain the referenced class prototypes of 4 key tissue types via conventional FCM from prior knowledge of referenced MR data. After data preparing, we construct PL model to obtain multiple 4-class classifiers. Global model is constructed as KT-CM and patches whose error impacts most become candidate patches, which need to be remodeled. Patch model is constructed as LapSVM, which is semi-supervised classification, and then updating the PL model. Finally, we organically combine multiple 4-class classifier to generate target synthetic CT image. Next, we detail each stages as follows.

3.1 Data Prepare

Feature extraction is of vital importance in machine learning and pattern recognition. The quality of features has a crucial impact on generalization performance. Considering the unavoidable noise in acquiring MR image, we adopt a principle of convolutional kernel to extract local texture features, which learns from the convolution layer in convolutional neural network (CNN) [10]. We extract local texture features from four types of abdominal MR data, i.e., fat, water, in-phase (IP) and opposed-phase (OP) [11], as the input to our SCG-PL method for each subject. Except for above features, position feature is adopted as well for better distinguish with the consideration of the similarity of signals of air and bone in MR data. The scan voxel size and pixel slices of 3D MR image are $0.98 \times 0.98 \times 5$ mm^3 and 512×512 pixel slices of Z-axis respectively. Considering isotropism, we design a grid partition strategy of 5×5 voxels assembled. Each voxel position feature is determined by spacing of size $4.9 \times 4.9 \times 5$ mm^3. Thus position feature (x, y, z) can be expressed as the indexes of grid, $1 \le x \le 103$, and $1 \le y \le 103$. Combining all the features we obtain seven dimension MR feature data as the input data to our method.

To generate final synthetic CT image from MR image as accurate as possible, we need referenced prior knowledge, i.e., referenced class prototypes of bone, air, fat tissue

and soft tissue. Thus, paired CT and MR images are necessary and each pair needed to deformably registered before. The work and data flows of Phase 2 are shown in Fig. Suppose there are n pairs CT and MR images to be referenced, we take one pair as example for detail. For reference pair 1, bone class centroid can be first determined since we can recognize bone data in MR image with CT data whose Hounsfield Unit (HU) is 300, and takes the average value of bone data as bone class centroid. Then we apply FCM to the leftover data, i.e., data without bone, for clustering and obtain three clusters centroids later. At this point, we obtain four class centroids of pair 1. And n referenced pairs produce n class centroids, class prototypes are the average value of class centroids for every class. Thus we obtain the reference class prototypes of four key tissue types.

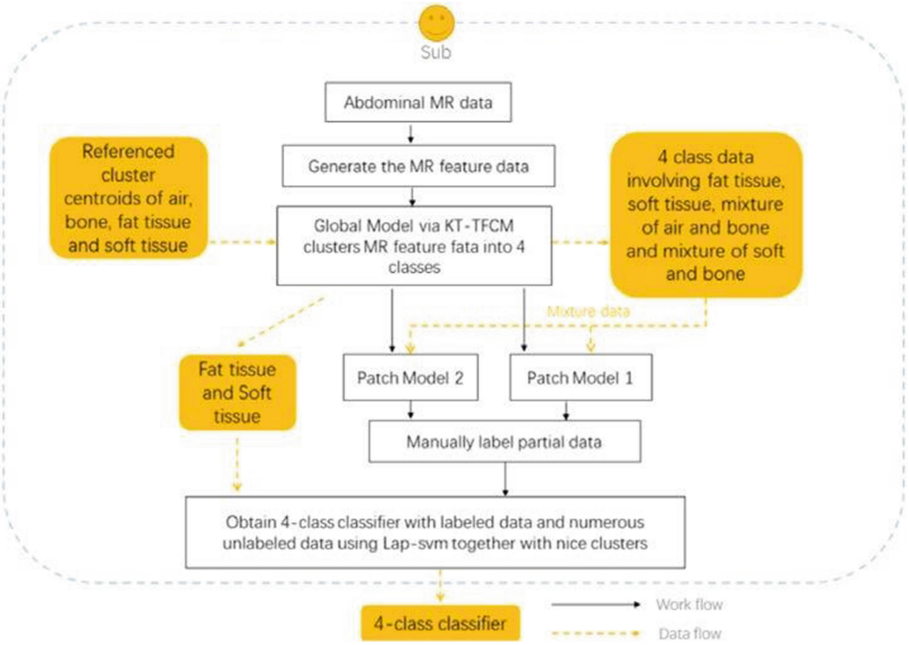

Fig. 2. Illustration of the work and data flows for generating 4-class classifier

3.2 Constructing PL Model to Obtain 4-Class Classifier

4-class classifier via PL model is necessary for generating synthetic CT, as shown in Fig. 2. Global model for constructing a 4-class classifier would naturally be KT-CM considering the existing historical referenced cluster centroids. The preliminary result of clustering would roughly be 4 classes, i.e., bone, air, soft tissue and fat tissue, after applying KT-CM to MR feature data. Owing to the fact that mDixon sequences are expert in reflecting fat tissue, the gained cluster of fat tissue after transfer clustering is relatively accurate. The leftover three clusters include soft tissue, bone and air. Soft tissue can be subdivided into one tissue approximate to soft bone and other soft tissue, which means soft bone and some soft tissue are mixed and hard to distinguish. In transfer clustering, the

cluster of soft tissue not close to soft bone is believable as well. Actually, the signals of air and hard bone are both very low in MR data thus one of the clusters from transfer clustering is the mixture of them.

In order to gain the final 4-class classifier to generate precise synthetic CT image, patch models are reconstructed in these mixture parts. Benefiting from the prior knowledge of subject's CT image, we can acquire labeled examples. However, it is practically infeasible for radiologist to label the whole data manually because of huge time consumption. Thus, semi-supervised classification can be used in patch model and LapSVM is ideal. With numerous unlabeled data and a limit amount of mark data, which is practically feasible for radiologist, it's capable of obtaining final 4-class classifier.

3.3 Generating Synthetic CT Image Through Multiple 4-Class Classifiers

We assemble multiple results of 4-class classifiers via the strategy of voting to decide voxel type. Considering numerous data in MR feature data, it's infeasible to directly take the entire data as input to our method because of huge time consumption. Thus, we propose sampling-KNN mechanism, which involves randomly sampling the MR feature data and using K nearest neighbor (KNN) to restitute the whole prediction results, in our method to accelerate the whole process. Sampling-size denotes as ss.

Specific CT value are set to 380, −700, 98 and 32 corresponding with bone, air, fat tissue and soft tissue with the referring to [12] to reconstruct a synthetic CT image.

4 Experiment Results

4.1 Setup

In this section, we assess the effectiveness of the proposed PL-TL-SC method for generating synthetic CTs. Thus, ten subjects were recruited using a protocol approved by the University Hospitals Cleveland Medical Center Institutional Review Board.

Moreover, three existing methods are in comparison with our method, i.e., the all-water method (AW) [13], transfer fuzzy C-means clustering (TFCM) and the support machine (SVM). Three metrics, i.e., the mean absolute prediction deviation (MAPD), the root mean square error (RMSE), and R [14, 15], are used to evaluate the effectiveness of our method.

We adopt Leave-one-out strategy to generate ultimate result. That is, we treat one subject as test dataset and the other leftover subjects as train dataset. Each result for generating synthetic CT of one subject are assembled from results of the remainder classifiers, which excludes the classifier of the test one.

Our experimental studies were carried out on a computer with an Intel i5-4590 3.3 GHz CPU, 8 GB of RAM, Microsoft Windows 10 (64 bit), and MATLAB 2017a.

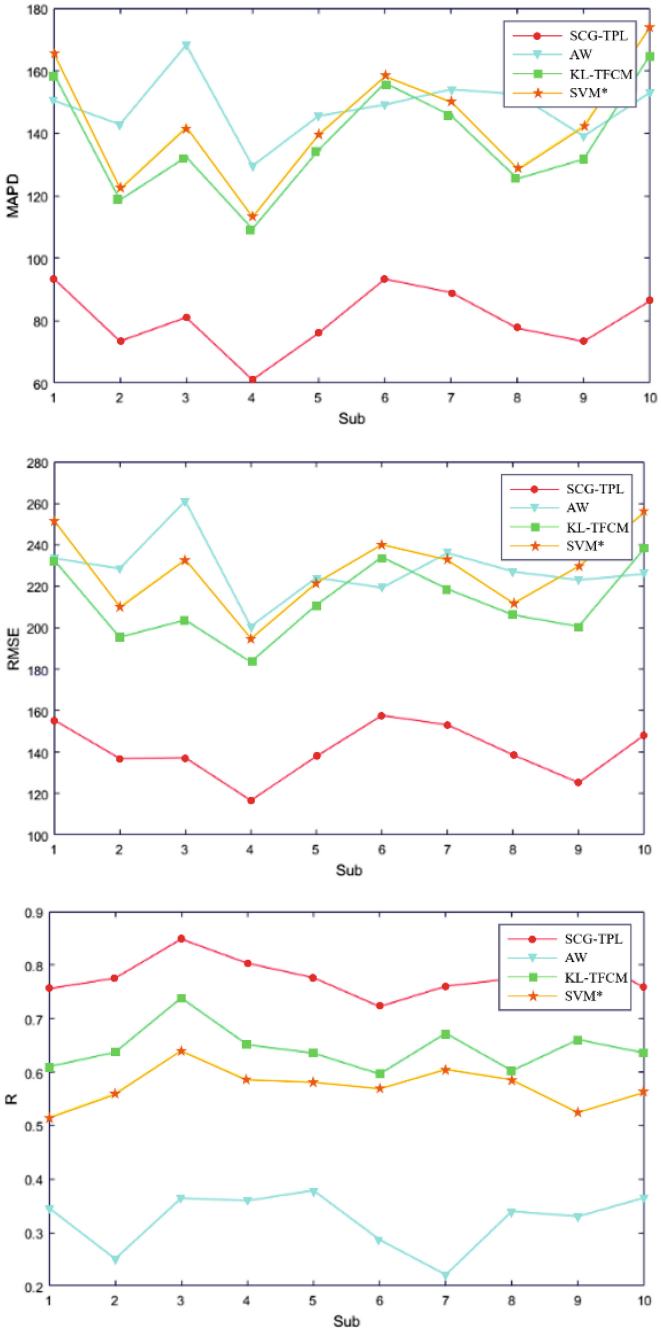

Fig. 3. Performance curves of the four methods. The proposed SCG-PL method has a lower mean absolute prediction deviation (MAPD), a lower root mean square error (RMSE), and a higher correlation (R) than the other three methods, including AW, TFCM and the SVM.

4.2 Results

We display the experimental results in Table 1 for each subject. In order to visually and intuitively present our method, the performance curves regarding to MAPD, RMSE and R metrics are shown in Fig. 2. As shown in Table 1, and we display the synthetic CT images from Sub8 with four methods above (Figs. 3 and 4).

Table 1. Performance comparison of generating synthetic CTS among the proposed SCG-PL and other methods

Sub	MAPD				RMSE				R			
	SCG-PL	AW	TFCM	SVM	SCG- PL	AW	TFCM	SVM	SCG-PL	AW	TFCM	SVM
1	**93.50**	150.45	159.02	165.59	**155.50**	233.49	232.64	251.39	**0.76**	0.35	0.61	0.52
2	**73.46**	142.80	118.63	122.24	**136.97**	228.49	195.38	210.21	**0.78**	0.25	0.64	0.56
3	**81.07**	168.21	132.39	142.04	**137.37**	261.03	203.70	232.85	**0.85**	0.36	0.74	0.64
4	**61.11**	129.55	109.36	113.25	**116.72**	200.63	183.44	194.80	**0.80**	0.36	0.65	0.59
5	**76.08**	145.55	134.63	139.75	**137.97**	224.10	210.92	221.79	**0.78**	0.38	0.64	0.58
6	**93.35**	149.09	156.05	158.22	**157.70**	219.24	234.02	240.17	**0.72**	0.29	0.60	0.57
7	**89.01**	154.07	145.61	150.10	**153.15**	235.96	218.61	232.73	**0.76**	0.22	0.67	0.61
8	**77.61**	152.41	125.44	128.56	**138.71**	227.09	206.17	211.88	**0.77**	0.34	0.60	0.59
9	**73.38**	139.04	131.70	142.41	**125.31**	222.99	200.56	229.57	**0.82**	0.33	0.66	0.52
10	**86.34**	153.00	164.96	174.12	**148.21**	225.90	238.13	255.79	**0.76**	0.37	0.64	0.56
Average	**80.49**	148.42	137.78	143.63	**140.76**	227.89	212.36	228.12	**0.78**	0.32	0.64	0.57

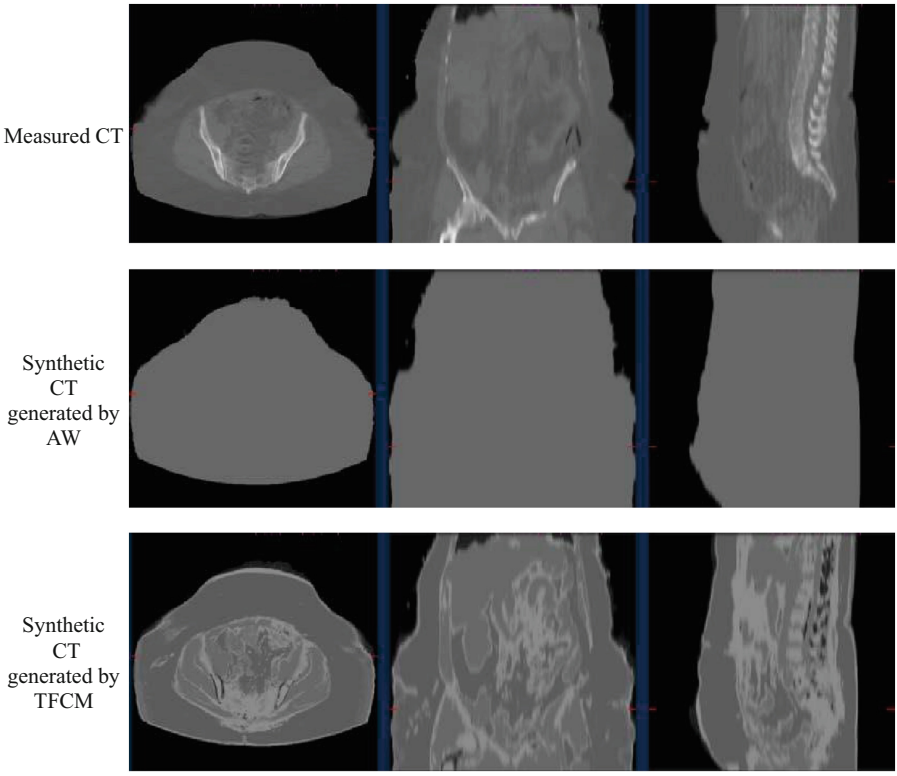

Fig. 4. Synthetic CT images on a representative subject (Sub 8) using four methods.

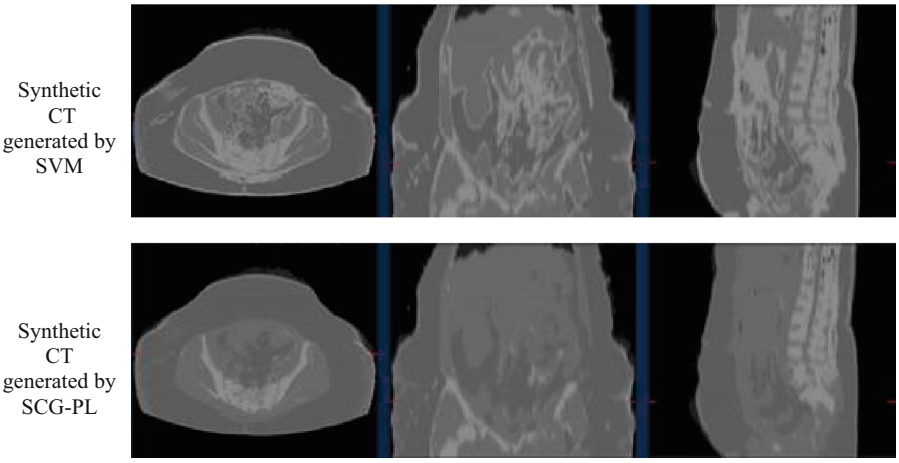

Fig. 4. (*continued*)

5 Conclusion

We study on the challenging abdominal section in medical image for generating synthetic CT image with mDixon MR image only. Recognizing the similarity between the situation we face and the feature of Patch Learning, we propose the effective SCG-PL method with techniques such as transfer learning for global model and semi-supervised classification for patch model. Patch Learning is a process of gradual improvement with remodeling indistinguishable domains to gradually obtain good performance of classification. This exactly corresponds the complicated situation in part of abdominal section because of deformable tissues and varying air position over time. The proposed method proves preferable generation of synthetic CT image.

References

1. Zaidi, H., Alavi, A.: Current trends in PET and combined (PET/CT and PET/MR) systems design. PET Clin. **2**(2), 109–123 (2007)
2. Zaidi, H., Mawlawi, O., Orton, C.G.: Simultaneous PET/MR will replace PET/CT as the molecular multimodality imaging platform of choice. Med. Phys. **34**(5), 1525–1528 (2007)
3. Hofmann, M., Steinke, F., Scheel, V.: MRI-based attenuation correction for PET/MRI: a novel approach combining pattern recognition and atlas registration. J. Nucl. Med. **49**(11), 1875–1883 (2008)
4. Farjam, R., Tyagi, N., Deasy, J.O.: Dosimetric evaluation of an atlas-based synthetic CT generation approach for MR-only radiotherapy of pelvis anatomy. J. Appl. Clin. Med. Phys. **20**(1), 101–109 (2019)
5. Kops, E.R., Herzog, H.: Template based attenuation correction for PET in MR-PET scanners. In: IEEE Nuclear Science Symposium Conference Record, pp. 3786–3789 (2008)

6. Liu, L., Cao, Y., Fessler, J.A.: A female pelvic bone shape model for air/bone separation in support of synthetic CT generation for radiation therapy. Phys. Med. Biol. **61**(1), 169–182 (2015)
7. Berker, Y., Franke, J., Salomon, A.: MRI-based attenuation correction for hybrid PET/MRI systems: a 4-class tissue segmentation technique using a combined ultrashort-echo-time/Dixon MRI sequence. J. Nucl. Med. **53**(5), 796–804 (2012)
8. Wu, D., Mendel, J.M.: Patch learning. IEEE Trans. Fuzzy Syst. **1906**, 00158 (2019)
9. Qian, P., et al.: Knowledge leveraged transfer fuzzy c-means for texture image segmentation with self-adaptive cluster prototype matching. Knowl.-Based Syst. **130**, 33–50 (2017)
10. Chen, Y., Jiang, H., Li, C.: Deep feature extraction and classification of hyperspectral images based on convolutional neural networks. IEEE Trans. Geosci. Remote Sens. **54**(10), 6232–6251 (2016)
11. Eggers, H., Brendel, B., Duijndam, A.: Dual-echo dixon imaging with flexible choice of echo times. Magn. Reson. Med. **65**(1), 96–107 (2011)
12. Schneider, W., Bortfeld, T., Schlegel, W.: Correlation between CT numbers and tissue parameters needed for Monte Carlo simulations of clinical dose distributions. Phys. Med. Biol. **45**(2), 459–478 (2000)
13. Andreasen, D., Edmund, J.M., Zografos, V.: Computed tomography synthesis from magnetic resonance images in the pelvis using multiple random forests and auto-context features. In: Medical Imaging: Image Processing. International Society for Optics and Photonics, vol. 9784, p. 978417 (2016)
14. Sekine, T., ter Voert, E.E.G.W., Warnock, G.: Clinical evaluation of zero-echo-time attenuation correction for brain 18F-FDG PET/MRI: comparison with atlas attenuation correction. J. Nucl. Med. **57**(12), 1927–1932 (2016)
15. Delso, G., Wiesinger, F., Sacolick, L.I.: Clinical evaluation of zeroecho-time MR imaging for the segmentation of the skull. J. Nucl. Med. **56**(3), 417–422 (2015)
16. Wen, J., Tian, Y., Yehang, S.: Improved evidential fuzzy c-means method. J. Syst. Eng. Electron. **29**(1), 187–195 (2018)
17. Tao, X., Wang, R., Chang, R.: Density-sensitive fuzzy kernel maximum entropy clustering algorithm. Knowl.-Based Syst. **166**, 42–57 (2019)